Soft Matter

ARTICLE TYPE

Electronic Supplementary Information for: Shape and Size Tunability of Sheets of Interlocked Ring Copolymers

Juan Luengo-Márquez, Salvatore Assenza, Cristian Micheletti

1 Linking modes in $P1$ and $P2$ lattices

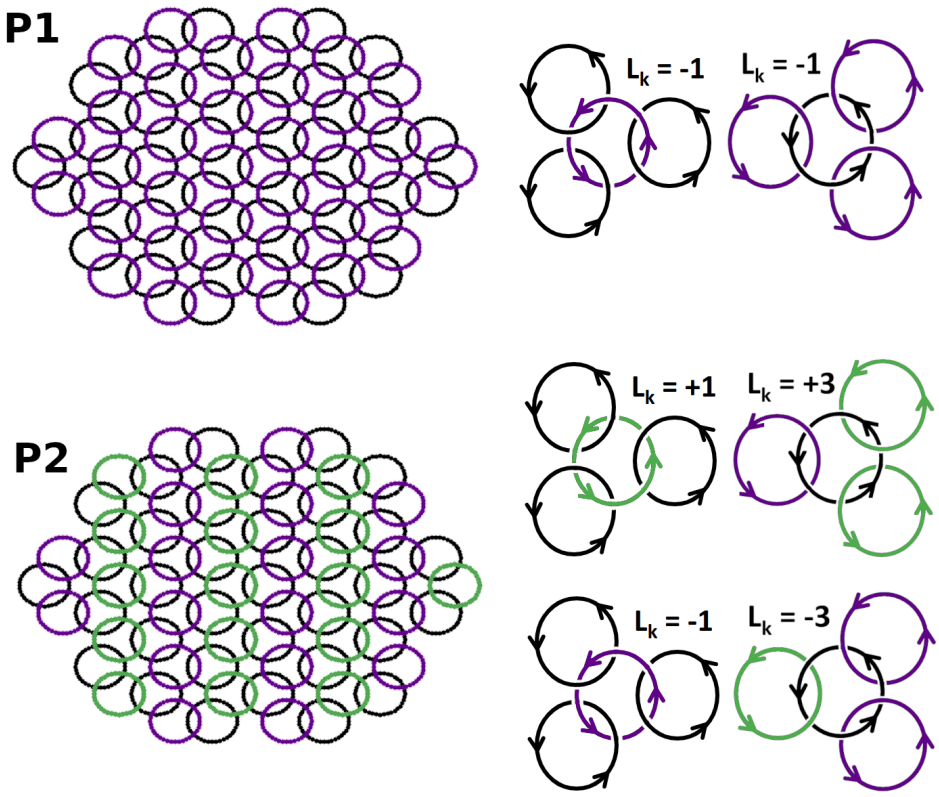

Fig. S 1 Shape and linking pattern of the catenated membranes with $n = 68$ rings. Linking number associated to each of the linking modes of every ring with three neighbors. The sketches on the right illustrate the convention used to orient the rings and associate a linking number to the central ring of three different local neigborhoods of P1 and P2 patches, after ref. [40] in the main text. In the broader context of a chainmail patch, each ring takes part to circular concatenated paths. The summed linking number of oriented rings in any such closed path is topologically conserved. This property makes P1 and P2 chainmails topologically inequivalent.

2 Simulation details and statistics

As described in the main text, for each ring composition and linking pattern, we run two simulations, with duration $2.5\times10^5\tau$ and $3.5\times10^5\tau$. These simulations were prepared by fixing the connectivity in the initial configuration with a homemade code, and then relaxing each of them independently via a soft potential

$$U_{soft}(r) = A\left[1+\cos\left(\frac{\pi r}{r_c}\right)\right], \qquad (1)$$

that describes the interaction between pairs of particles at a distance $r < r_c$, where $r_c = 1\sigma$ is the cutoff radius and $A = 1\varepsilon$ is the energy constant. This relaxation is meant to avoid overlaps between atoms before initiating the Langevin dynamics simulation.

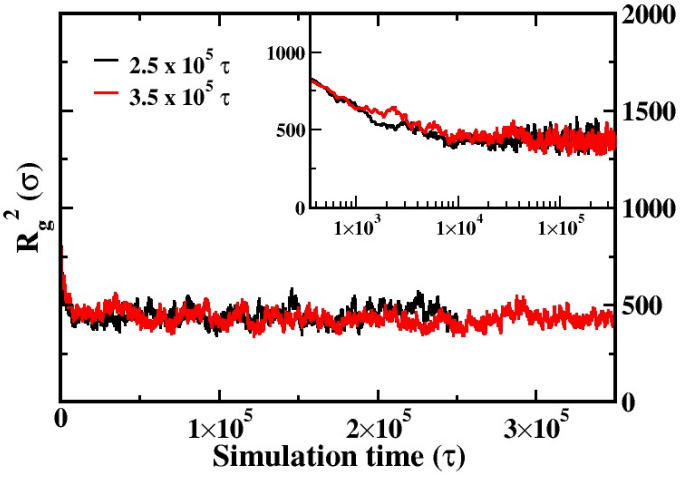

Fig. S 2 Characteristic relaxation times: For each composition and linking pattern, we first run a $2.5\times10^5\tau$ simulation. We then test the convergence of the measured properties running a simulation of $3.5\times10^5\tau$. Here we show as an example the global R_g^2 of the fully rigid composition with $P1$. The inset displays the logarithmic scale. The relaxation time is roughly $5\times10^4\tau$, which is the time that we discarded for the analysis.

For the properties presented in this work (μ), and except otherwise indicated, we first compute the average of that property for each independent simulation ($\mu_1 =< \mu >_{2.5\times10^5\tau}$ and $\mu_2 =< \mu >_{3.5\times10^5\tau}$). Then the value presented is the average between them ($\bar{\mu} = \frac{1}{2}(\mu_1+\mu_2)$) and the error bars are the corresponding standard error

$$\sigma = \sqrt{\frac{[(\mu_1-\bar{\mu})^2+(\mu_2-\bar{\mu})^2]}{2}} = \frac{|\mu_1-\mu_2|}{2}. \qquad (2)$$

We check the reliability of these error bars by computing, for the metric properties of the whole membranes (R_g and eigenvalues of the gyration tensor), the averages and errors using a different procedure. We split the trajectories in blocks of $10^5\tau$, which corresponds to roughly twice the relaxation time of R_g, and compute the average for each of the blocks. From the resulting 5 independent data points (first $5\times10^4\tau$ are still discarded), we compute then the average and the standard error of the mean.

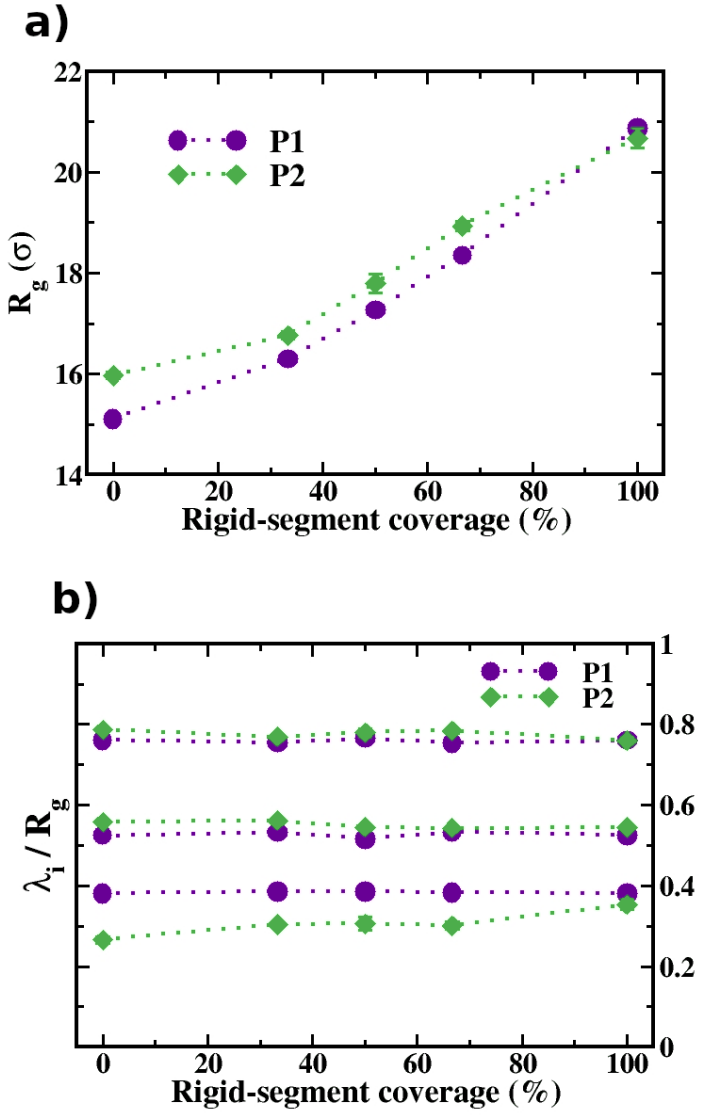

Fig. S 3 Global metric properties with alternative error calculation. a) R_g of membranes. b) Ranked gyration tensor eigenvalues.

The resulting error bars for the global metric properties (Fig. 3) are visually indistinguishable from those represented in Fig. 4 of the main text.

The properties associated to isolated rings were computed in a different manner, as only one simulation of duration $2.5\times10^5\tau$ for each composition was carried out. In this case, we used a combination of block analysis and bootstrap-

ping, a procedure intended to maximize statistical reliability. The set of instantaneous values of the target property computed during the simulation is split in blocks of the same size, and for each block, we compute the average of the property and run bootstrap analysis on these averages to get the error. This process is repeated for several block sizes, until convergence in the subsequent error is achieved.

3 Average mechanical bond length

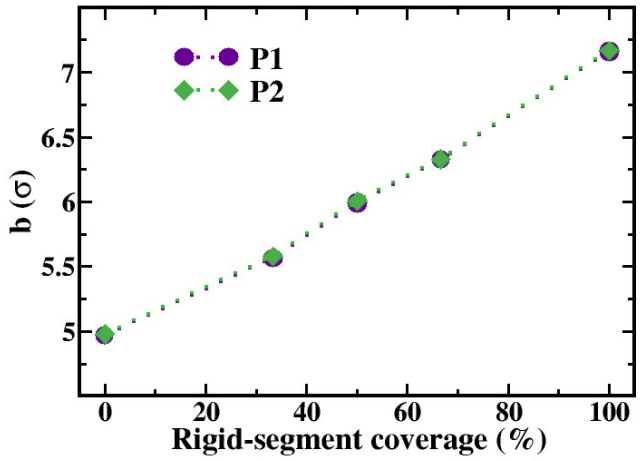

Fig. S 4 Average mechanical bond length for both linking patterns: distance between centers of linked rings. Error bars are present, although smaller than the symbols. The errors are computed as the estimate of the standard error of the sample mean considering the average values from the simulation of $2.5 \times 10^5 \tau$ and the one of $3.5 \times 10^5 \tau$.

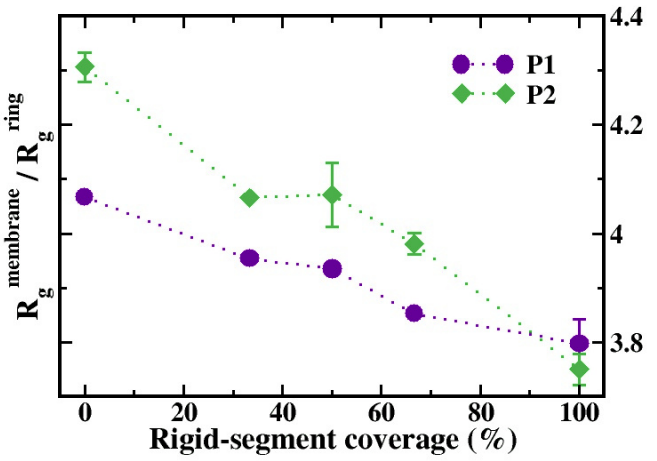

Fig. S 5 Ratio R_g of membranes with R_g^{ring}, computed for rings within membranes with the same linking pattern. Even after discounting the effects related to the size of individual rings, the largest differences between P1 and P2 membranes are for the fully flexible rings. Error bars are computed as the estimate of the standard error of the sample mean considering the average values from the simulation of $2.5 \times 10^5 \tau$ and the one of $3.5 \times 10^5 \tau$.

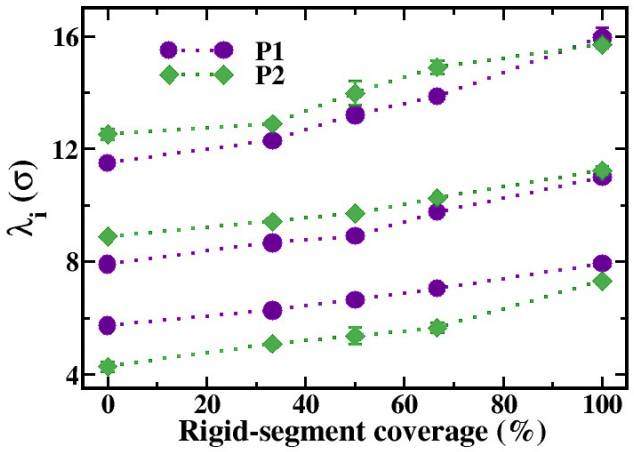

Fig. S 6 Eigenvalues of the gyration tensor of the whole membranes ($\lambda_1^2 > \lambda_2^2 > \lambda_3^2$) without normalization ($\sqrt{<\lambda_i^2>}$). Error bars are computed as the estimate of the standard error of the sample mean considering the average values from the simulation of $2.5 \times 10^5 \tau$ and the one of $3.5 \times 10^5 \tau$.

5 Shape of single rings

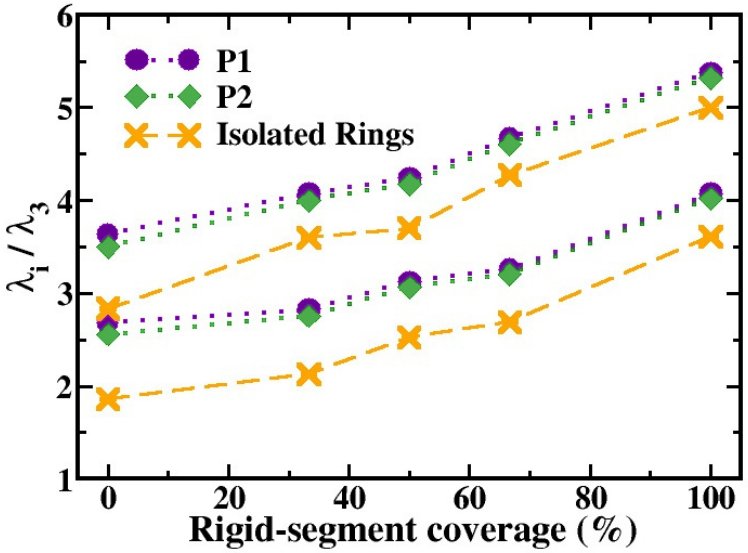

Fig. S 7 $\sqrt{<\lambda_i^2>/<\lambda_3^2>}$ for $i = 1,2$ of single rings. Rings within membranes with $P1$ (violet dots) and with $P2$ (green diamonds) do not differ significantly, as it is generally the case for local properties. Both seem stretched when compared to isolated rings (orange crosses), whose λ_1 and λ_2 are closer to λ_3. As expected, this stretching effect is less important in the case of fully rigid rings. Error bars are present, although smaller than the symbols. The errors in $P1$ and $P2$ are computed as the estimate of the standard error of the sample mean considering the average values from the simulation of $2.5 \times 10^5 \tau$ and the one of $3.5 \times 10^5 \tau$. The errors for the isolated rings are computed with block analysis and bootstrapping.

6 Model for contacts among particles

Here we show a detailed derivation of Eq. 7 in the main text. For any given pair of interlocked rings, we consider the different costs in conformational energy ΔF_{ij} associated with any combination of contacts, using as a reference each isolated ring

$$\begin{aligned}\Delta F_{ff} &\equiv \Delta F_f + \Delta F_f \ , \\ \Delta F_{fr} &\equiv \Delta F_f + \Delta F_r \ , \\ \Delta F_{rr} &\equiv \Delta F_r + \Delta F_r \ , \end{aligned} \tag{3}$$

where ΔF_i is the change in conformational free energy of a ring whenever it exposes a particle of type i as a contact with another ring. Therefore, in Eq. 3, we have assumed that the free energy of a contact is a simple addition of free-energy changes associated with each of the fragments establishing the contact, independently of the nature of the partner fragment.

We can then define the excess free energy $\Delta F \equiv \Delta F_f - \Delta F_r$ as the net free-energy change associated with a contact established by a *flexible* particle as compared to a *rigid* one. We also define x as the fraction of rigid particles over the total number of particles per ring ($0 \leq x \leq 1$).

Then the probability of each type of contact is proportional to the probability of a random sampling (assuming that the number of particles is large) times a Boltzmann factor accounting for the statistical weight of each sampling

$$\begin{aligned} P_{ff}(x) &\propto (1-x)^2 \exp\left(-\frac{\Delta F_{f-f}}{k_B T}\right) = (1-x)^2 \mu^2 \omega^2, \\ P_{fr}(x) &\propto 2x(1-x) \exp\left(-\frac{\Delta F_{f-r}}{k_B T}\right) = 2x(1-x)\mu^2 \omega, \\ P_{rr}(x) &\propto x^2 \exp\left(-\frac{\Delta F_{r-r}}{k_B T}\right) = x^2 \mu^2, \end{aligned} \tag{4}$$

where the last expression of each appears after substituting the corresponding free energy change with its definition in Eq. 3 and then applying the definitions

$$\mu \equiv \exp\left(-\frac{\Delta F_r}{k_B T}\right), \qquad \omega \equiv \exp\left(-\frac{\Delta F}{k_B T}\right). \tag{5}$$

Eq. 7 in the main text follows after normalizing all probabilities in Eq. 4 with $P_{ff}(x) + P_{fr}(x) + P_{rr}(x) = \mu^2 \left[(1-x)^2 \omega^2 + 2x(1-x)\omega + x^2\right]$.

7 Contacts between ring pairs

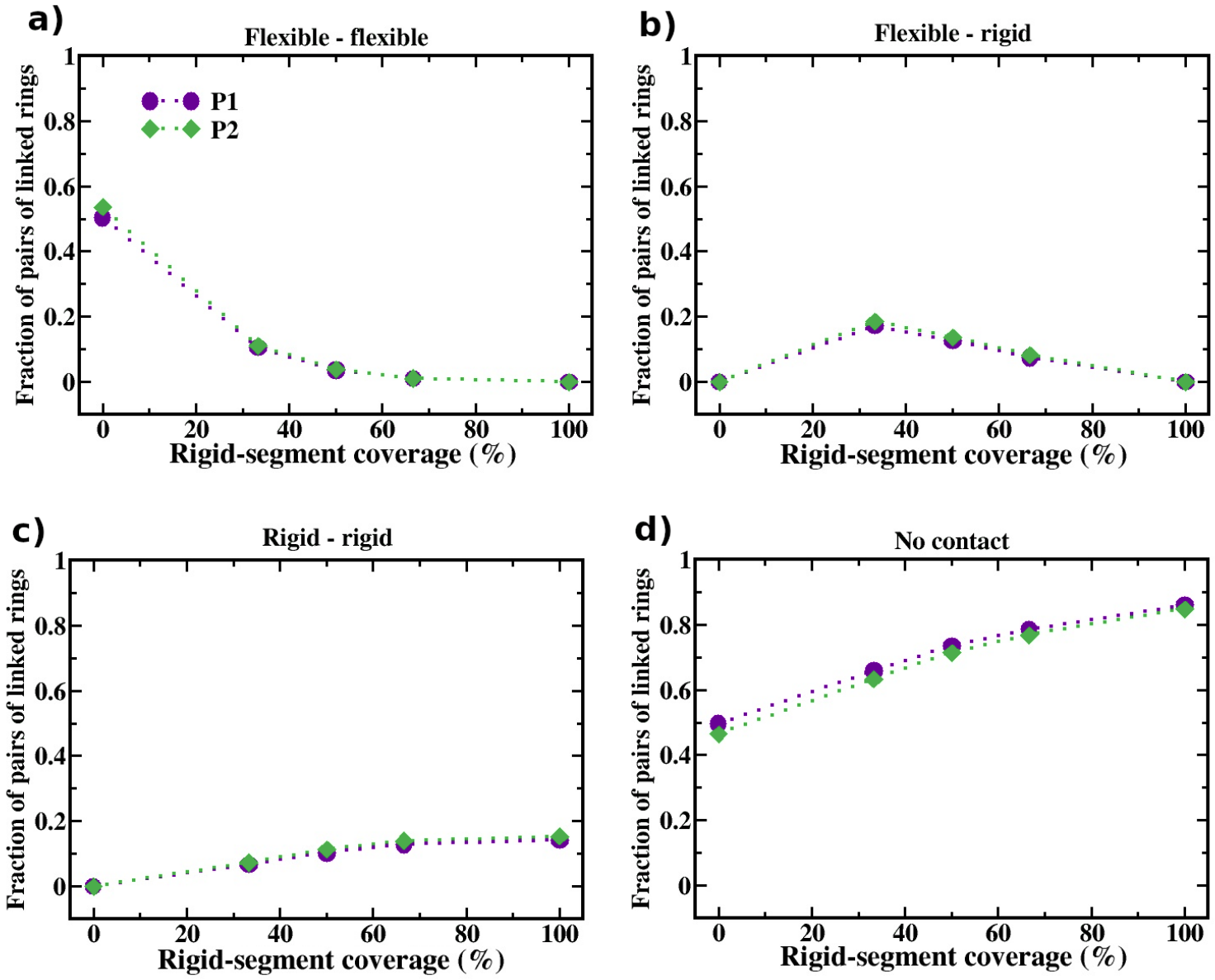

Fig. S 8 Fraction of ring pairs having a) flexible-flexible contact, b) flexible-rigid contact, c) rigid-rigid contact, and d) no contact. For each pair of linked rings, we identify the pair of particles — belonging to each of the rings — i) whose distance is smaller than $\sqrt[6]{2}\sigma$, and ii) which are closer to each other. We assign the type of contact depending on the particle type. If no pair of particles for a given ring pair fulfills the conditions i) and ii), we assign "no contact". The errors are computed as the estimate of the standard error of the sample mean considering the average values from the simulation of $2.5 \times 10^5 \tau$ and the one of $3.5 \times 10^5 \tau$.

8 Instantaneous K_G heatmaps

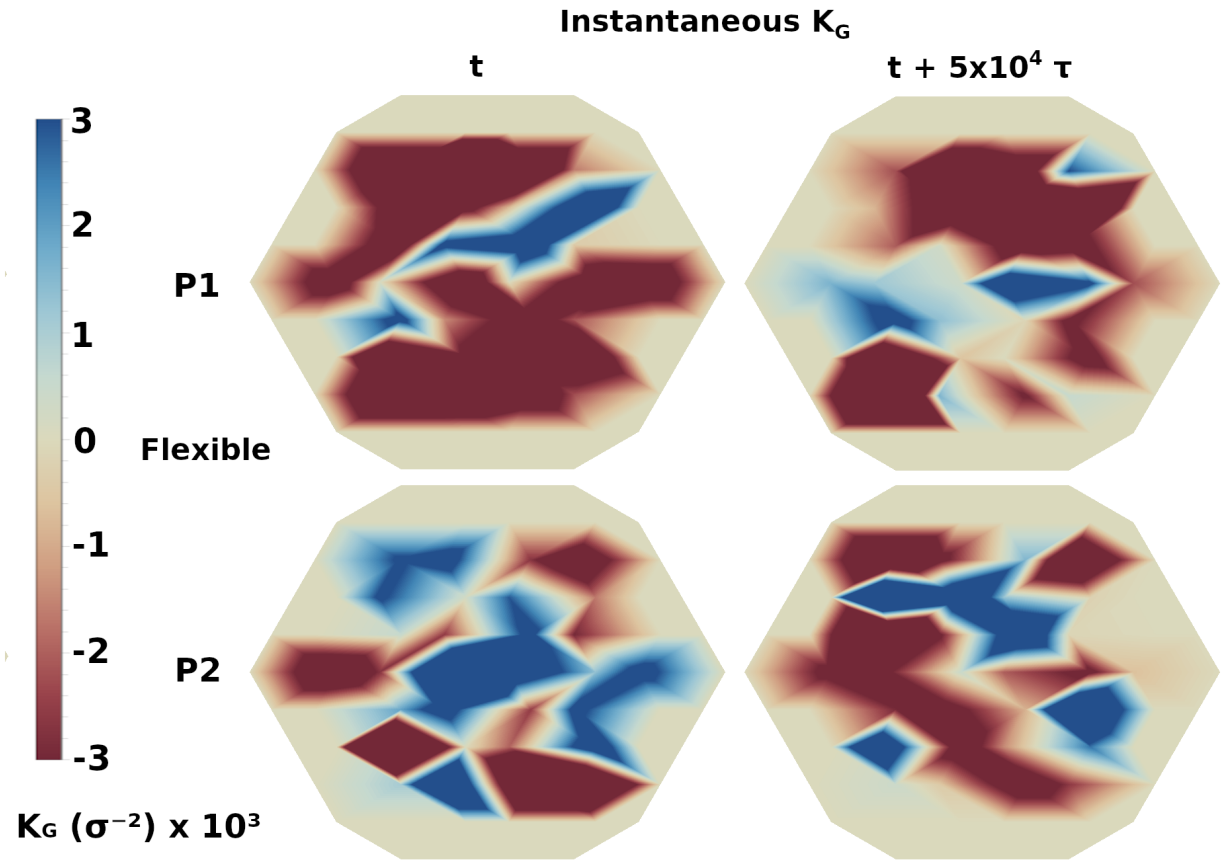

Fig. S 9 Instantaneous K_G heatmaps using the $2.5 \times 10^5 \tau$ simulation of the fully-flexible composition. Top line corresponds to P1 chainmails, while bottom line are P2 chainmails. For each linking pattern, we show the K_G per vertex of two frameshots separated a time $5 \times 10^5 \tau$, similar to the typical autocorrelation time of the gyration radius of the chainmails. The legend bar is saturated for better visualization.

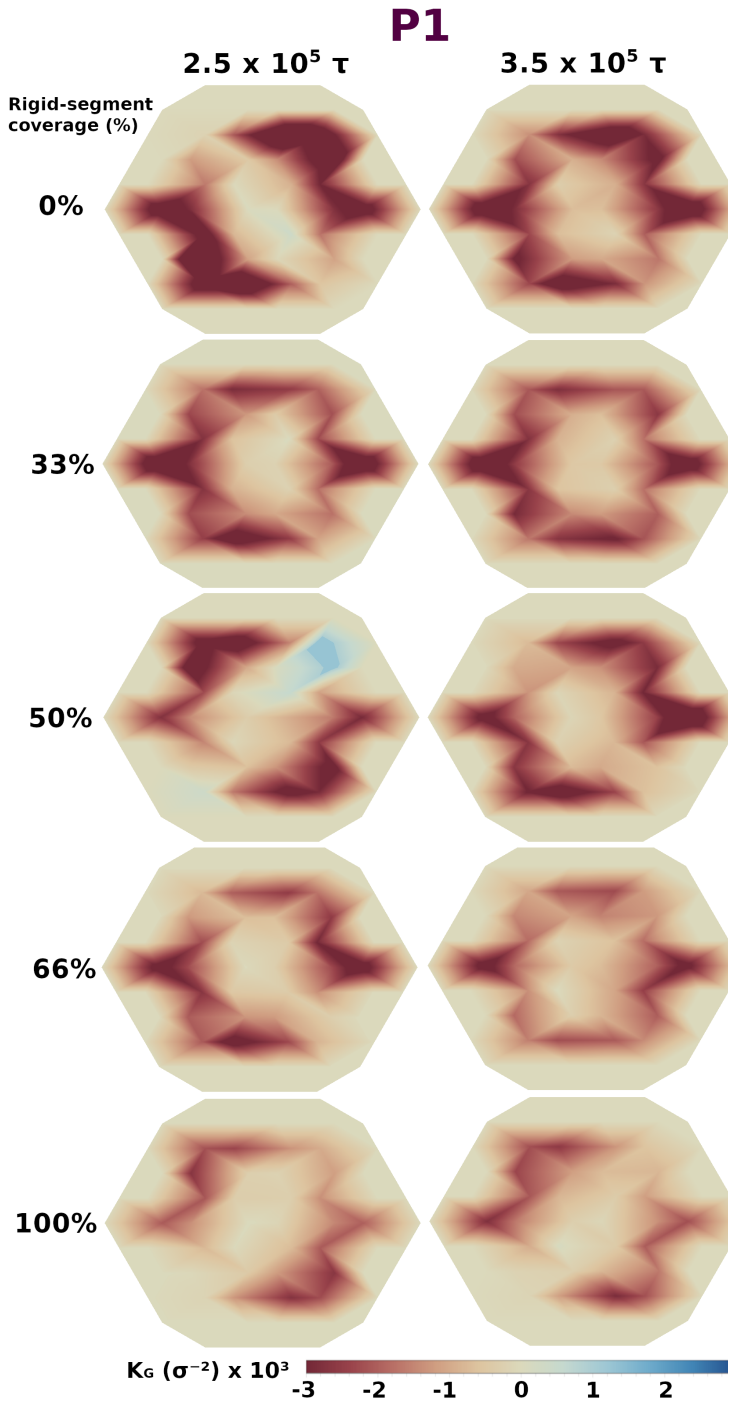

Fig. S 10 K_G per vertex for $P1$ membranes at all compositions. Left column displays the $2.5 \times 10^5 \tau$ simulation and right column the $3.5 \times 10^5 \tau$ simulation. In the 50% case, the line with more negative values of K_G has different inclinations, pointing out a spontaneous symmetry breaking. The legend bar is saturated in the negative side for better visualization.

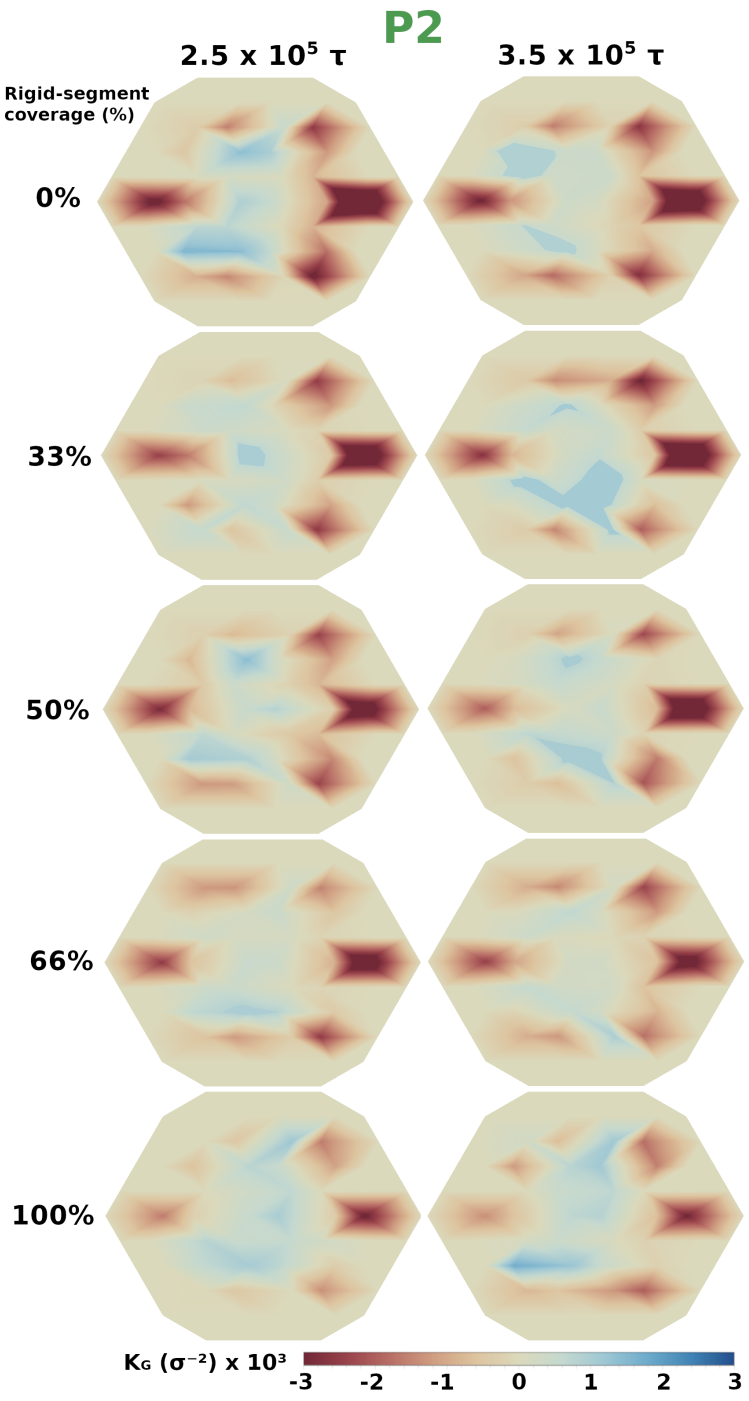

Fig. S 11 K_G per vertex for $P2$ membranes at all compositions. Left column displays the $2.5 \times 10^5 \tau$ simulation and right column the $3.5 \times 10^5 \tau$ simulation. The legend bar is saturated in the negative side for better visualization.

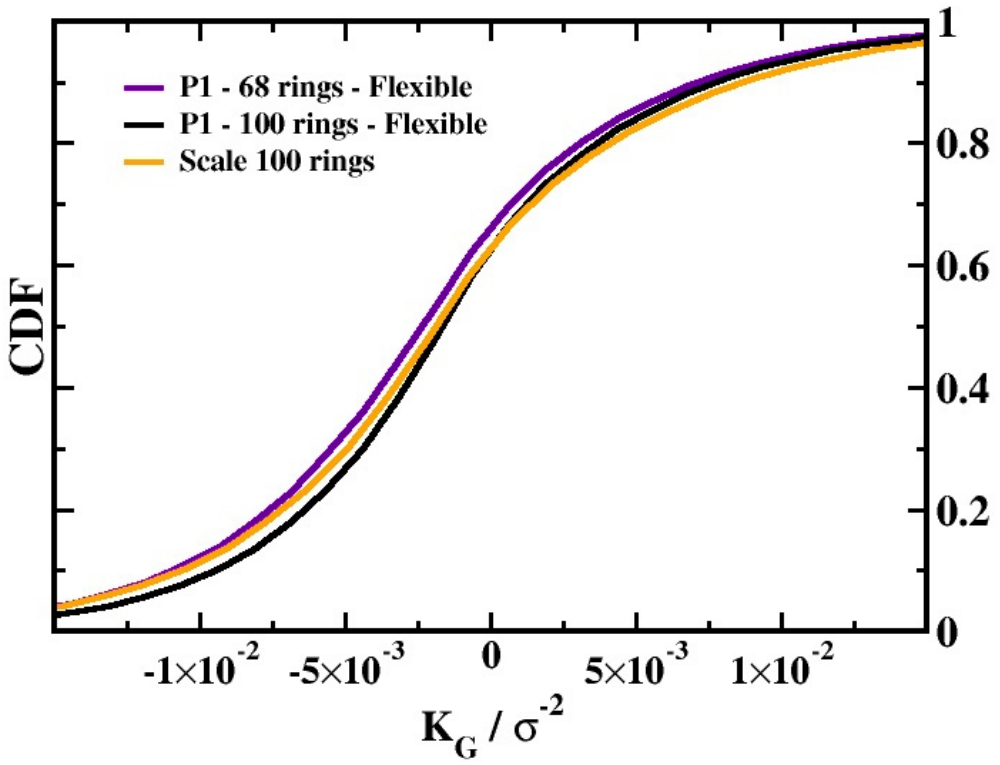

Fig. S 12 Curvature scales with membrane size. Cumulative Density Functions (CDFs) of K_G for fully flexible $P1$ membranes with 68 rings (violet dots) and 100 rings (black line). Orange line represents the re-scaled distribution of the black line with $q = 1.06 \pm 0.04$. The scaling factor was computed minimizing the quadratic error of the re-scaled PDF relative to the PDF of the membrane with 68 rings, and its error span the values of q that provide a quadratic error under 5% relative to the peak of the reference distribution.